Journal of Thermal Analysis and Calorimetry, Vol. 97 (2009) 1, 27–32

# TEMPERATURE-INDUCED CHANGES IN CRYSTAL LATTICE OF BIOARAGONITE OF *TAPES DECUSSATUS LINNAEUS* (MOLLUSCA: *BIVALVIA*)

*J. Nemliher*[1], *K. Tõnsuaadu*[2*] *and T. Kallaste*[1]

[1]Institute of Geology, Tallinn University of Technology, Ehitajate tee 5, 19086, Tallinn, Estonia
[2]Laboratory of Inorganic Materials, Ehitajate tee 5, 19086, Tallinn, Estonia

The characteristics of bioaragonite of shells of recent *T. decussatus* during heating were studied by the means of TG-DTA-EGA (FTIR), XRD, XRF and FTIR. The mass loss recorded up to 2.5% appeared with the higher rates at 110–150, 200–250, 295–300, and 390–415°C at heating of 10°C $min^{-1}$ up to 500°C. IR analysis of the evolved gases revealed the emission of water and $CO_2$. The lattice constants tend to change with anisotropy character (parameters *a* and *c* diminish whilst *b* tends to grows) and with an overall contraction of cell volume (from 227.36 to 226.84 $Å^3$) during heating was established. The peculiarity of bioaragonite was explained by substitution of $H_2O$ and sulphate ion into the lattice. In spite of those substitutions, bioaragonite reveals an orthorhombic structure, which is preserved during the changes up to calcite formation above 380°C.

***Keywords:*** *bioaragonite, crystal structure change, structural substitutions, TG/DTG/DTA/TG-FTIR*

## Introduction

Together with calcite, a trigonal $CaCO_3$, the orthorhombic polymorph of Ca-carbonate, aragonite, is one of the most widespread biominerals, formed during the matrix biomineralization process [1]. Aragonite constitutes an important part of the material for limestone formations. During the transition of carbonate mud into limestone, aragonite transforms into calcite. This process proceeds at low temperatures, consequently, excitation of this transformation should be connected with a nature of bioaragonite. The heating of a biomineral is reported as a good tool for the modelling of fossilization [2].

Thermally induced transformation of Ca-carbonate phases is a well-studied matter in the case of geological aragonites [3] as well as bioaragonites [4]. Considering the thermal behaviour of bioaragonite of bivalves, the main attention has been devoted to the details of aragonite–calcite transition [5], especially with respect to the organic compound impact on this process [6]. The shift of the aragonite–calcite transformation temperature from 250 to 500°C has been attributed to cationic substitutions [7] and hydration of aragonite [4, 8, 9].

In the orthorhombic structure, ions of Ca, being in the IX coordination, tend easily to be substituted by Sr, a phenomenon that might be treated as having a taxa-specific character. So, the highest Sr content in bioaragonites has been reported in coral biomineral [10] with an observable water temperature-dependent Ca/Sr ratio [11]. A more moderate Sr content has been reported to be characteristic of molluscan bioaragonite, snails and bivalves [12].

Another important substitution into bioaragonite lattice is a water molecule, assumed by Passe-Coutrin [4] and proved by Verma [13]. Basically, there exist two structural forms of hydrated Ca-carbonates: trigonal (rhombohedral) monohydrocalcite $CaCO_3 \cdot H_2O$ [14], and monoclinic ikaite, $CaCO_3 \cdot 6H_2O$ [15]. In both, the water is involved in a Ca-carbonate structure via hydrogen bonding. The first might be treated as a hydrated modification of calcite, and the second as a hydrated modification of aragonite (with lowered symmetry). Both have been reported to tolerate the substitutions in cation position, such as Sr, Na, Fe and Mg. The recent works of Verma [13] show clearly the unisotropy character of water substitution into bioaragonite lattice. The thermal behaviour of different types of water, bound into minerals, has been well discussed by Földavari [16], revealing that TA is a suitable method to distinguish the different bonding manners.

In this work, an attempt to clarify the low-temperature changes of bioaragonite with respect to lattice changes, thermal effects and evolved gas composition is made.

## Experimental

### *Materials*

Subfossil shells of *Tapes decussatus* were collected on the shore of the Irish Sea near Carnarfon, Wales. The shells were cleaned of periostracum by 50% $H_2O_2$, washed in distilled water, dried and shattered into

* Author for correspondence: kaiat@staff.ttu.ee

1388–6150/$20.00

Akadémiai Kiadó, Budapest, Hungary
Springer, Dordrecht, The Netherlands

particles about 1–2 mm in diameter. Further mechanical grinding was avoided in order to prevent the transition of aragonite into calcite. The organic matter of the shell was removed in an agitator vessel by 15% $H_2O_2$ solution, buffered by $NH_4OH$, at room temperature until white powder formation. The pH of the solution was kept permanently alkaline. Principally, the peroxide treatment of shell bits models well the post mortem development of bioaragonite – in nature, shells are subjected to mechanical grinding by undulation and organic matter oxidation.

The residual matter was washed in distilled water, dried at 60°C and divided into two parts. One part of this material was subsequently heated in a furnace up to temperatures of 110, 130, 150, 170, 190, 210, 230, 280, 330 and 380°C; the material was kept for a duration of 1 h at each temperature. The heated and unheated material was analysed by means of TA, FTIR, XRD and XRF.

*Methods*

TA-FTIR

For thermal analysis a Setaram LabSys 2000 instrument was used. A TG/DTA analysis was carried out at a heating rate of 10°C $min^{-1}$ in an air or $N_2$ flow of 50 mL $min^{-1}$ in an open Pt crucible, with a sample mass of ~30 mg. In the TG/EGA experiments (sample mass ~400 mg, gas flow 100 mL $min^{-1}$), the on-line gas composition was monitored using an FTIR gas analyser (Interspectrum). The Ranger-AlP Gas Cell S/N 23790 (Reflex Analytical Co.) with 8.8 meters' path length was maintained at 150°C. Spectra were recorded in the 600–3500 $cm^{-1}$ region with a resolution of 4 $cm^{-1}$ and 4 scans per slice.

The gases evolved were identified using characteristic infrared absorption wavelengths: for $NH_3$ at 930 and 963 $cm^{-1}$, $H_2O$ at 1520–1700 and $CO_2$ at 2354 and 2358 $cm^{-1}$ [17]. The profiles of the evolvement of gases were obtained as temperature derivatives of the peak area integrated above the baseline from 900 to 980 $cm^{-1}$ for $NH_3$, from 1520 to 1700 $cm^{-1}$ for $H_2O$ and from 2227 to 2418 $cm^{-1}$ for $CO_2$.

XRF

The content of Na, Sr, S, P and Br was analysed by X-ray fluorescence from pressed-powder pellets using the standard technique and a VRA-30 XRF analyser.

XRD

The material was powdered in an agate mortar, mixed with about 15% of Si (internal standard) and prepared using alcohol. XRD patterns were obtained on a diffractometer HZG-4. The samples were scanned at a step of 0.02° within the range of 28–70° of 2θ, which covered 27 aragonite, 3 silicon and 11 calcite reflections. Fe-filtered Co radiation ($\lambda K\alpha_1$=1.788965Å) was used. Each point was measured for a duration of 5 s. The lattice parameters were calculated using the whole-pattern fitting technique via the refinement of lattice parameters of aragonite and with fixed values for calcite. The measured XRD reflections were fitted by the sum of two modified Lorentzian profile-shape functions for reflections of silicon ($K\alpha_1$ and $K\alpha_2$) and by the sum of two Lorentzian profile-shape functions for aragonite and calcite [18]. The peak-shift error was corrected on a 2θ scale, using silicon reflections. The linear dependence of the 2θ shift was assumed over the measured angular range. Because of the low content of calcite, the pattern for that mineral was modelled from the Iceland spar standard. For aragonite, the lattice parameters, reflection intensities and their half-widths were refined. In order to reduce the number of free parameters, the reflections were divided into 3 groups. As the main broadening of peaks was found to be related to the 010 crystallographic direction, the value of cosϕ (where ϕ is the angle between the 010 lattice direction and particular lattice direction) was taken for the division into groups, with values of cosϕ 0–0.5, 0.5–0.8 and 0.8–1, respectively.

Based on the remeasuring of the same sample, the measurement error might be estimated as 0.0005 Å for *a* and *c* lattice parameters and 0.002 Å for the *b* lattice parameter.

## Results and discussion

The shells of *Tapes decussatus* are found to be fully aragonitic (Fig. 1). In addition to the basic constituents ($CaCO_3$) the sample contains 0.67% $Na_2O$, 1810 ppm Sr, 1890 ppm S, and <3 ppm Br.

*Thermal analysis*

Thermogravimetric analysis curves (Fig. 2a) show that the mass loss of shell bits or peroxide-treated powder starts at 80°C and reaches 2.48% in the air flow and 2.31% in the $N_2$ flow at 500°C. The mass loss difference is about 0.8% for peroxide-treated material, which indicates the rate of organic matter removal.

In the DTG curves (Figs 2b–d), four overlapping reactions could be differentiated with the maximum rates in the temperature intervals 110–150, 200–250, 295–300 and 390–415°C. The exact position of the DTG peak tops depends on the sample and the atmosphere of the experiment.

A comparison of the DTA curves of the shell bits and those of the peroxide-treated material in the air

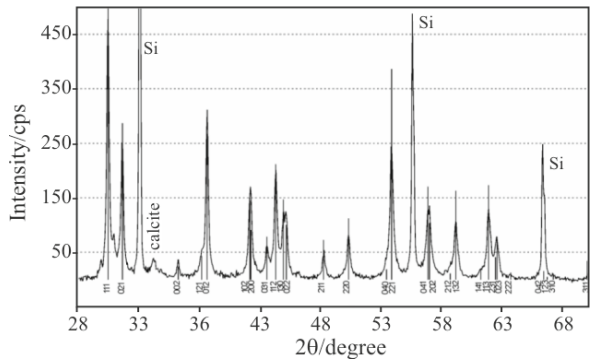


**Fig. 1** XRD pattern of bioaragonite, heated at 210°C for 1 h

flow reveals an exothermic effect with a peak top at 310°C (Fig. 2e) that does not appear in the $N_2$ atmosphere. This oxidation reaction is proof of the organic matter in the shell structure that decomposes partially at heating up to 500°C [19]. Most of this organic matter was removed by treatment with peroxide solution. The endothermic effect corresponding to the aragonite→calcite transformation at 400–430°C [16] is not clearly visible. Therefore, the amount and the conditions of decomposition of organic matter in bioaragonite impact on the thermal transformations.

IR analysis of the evolved gases during heating reveals the emission of water and $CO_2$ (Fig. 3). Traces of $NH_3$ were also detected in the case of the organic-rich sample (shell bits). The evaporation of water starts at about 80°C in all the experiments and has a similar profile with the DTG curve up to 250°C (Figs 2b–d). The release of water ends in the peroxide-treated sample at 300°C and in the bits at a temperature 30°C higher.

By the profile of $CO_2$ in the gas phase its extensive emission starts at about 200°C, having the maximum rate at 300°C, and finishes at 400–420°C. The maximum $CO_2$ emission coincides with the exothermic effect in the air. These results testify to the pyrolysis of the organic matrix in the shell structure at heating.

The evolvement of water before the decomposition of organic matter occurs due to the evaporation of adsorbed water in the interval 80–150°C and of structural water at 150–250°C [16]. At temperatures above 250°C, the evolvement of water occurs additionally due to the pyrolysis reaction.

*FTIR spectroscopy*

The spectra of starting materials reveal a decrease in organic matter content as a result of treatment with hydrogen peroxide (Fig. 4): the intensity of the peaks at 1630 $cm^{-1}$ and in the intervals 2800–3000 (not shown in Fig. 3) and 3200–3500 $cm^{-1}$, attributed to organic matter, decrease. A lack of peptides in $H_2O_2$-treated matter explains the missing of $NH_3$ spectral lines in the evolved gases spectra.

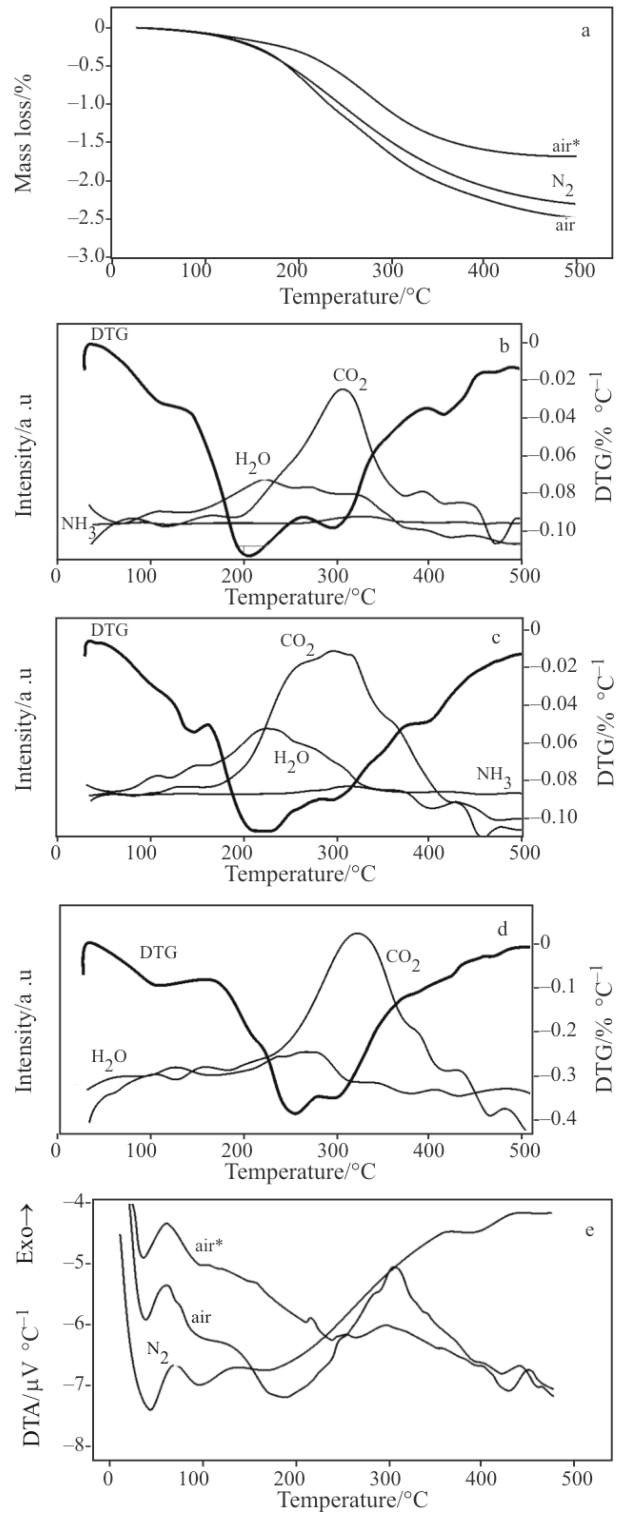


**Fig. 2** Curves of thermal analyses: a – mass change of the shell bits in the air (*$H_2O_2$ treated shell) and $N_2$; b – DTG and $CO_2$, $H_2O$ and $NH_3$ evolvement profiles of shell bits in the air; c – DTG and $CO_2$, $H_2O$ and $NH_3$ evolvement profiles of $H_2O_2$ treated shells in the air; d – DTG and $CO_2$, $H_2O$ and $NH_3$ evolvement profiles of shell bits in $N_2$; e – DTA of the shell bits in the air (*$H_2O_2$ treated shell) and $N_2$

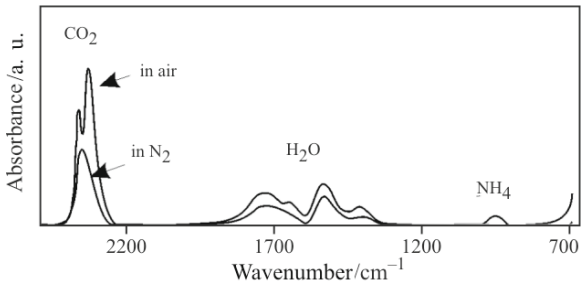


**Fig. 3** IR spectra of evolved gases at 300°C: 1 – shell bits in the air; 2 – peroxide treated sample in $N_2$

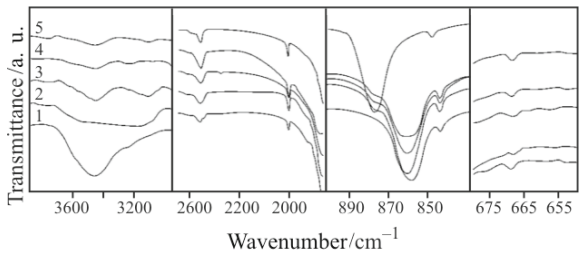


**Fig. 4** IR spectra: 1 – shell; 2 – peroxide treated sample; and samples after calcination at 3 – 210; 4 – 330; 5 – 430°C

In the spectra of the calcined samples are visible absorption bands assigned to calcite ($\nu_2$ 875, $\nu_3$ 1430 $cm^{-1}$) alongside the bands of aragonite ($\nu_1$ 1083, $\nu_2$ 857, $\nu_3$ 1490, $\nu_4$ 700 and 713 $cm^{-1}$) [5] starting from 170°C. Only the bands belonging to calcite could be found above 380°C.

The intensity of bands, characteristic of moisture or chemically bound water (OH vibrations at 3000–3600 $cm^{-1}$), decreases gradually with a temperature increase.

Additionally to these well-identified peaks, some very weak peaks (relative intensity 3–5%) are found at 540, 568, 606, 669, 726, 876 and 909 $cm^{-1}$. As different substitutions are found in the structure of biominerals [4, 6, 8–10] their identification is complicated. Nevertheless, we suppose that the absorption band at 669 $cm^{-1}$ belongs to sulphate [20], most likely introduced into the bioaragonite structure. The carbonate bands hide the other vibrations of sulphate at 1018–1120 and 598–610 $cm^{-1}$.

*XRD*

The XRD pattern of bioaragonite is shown in Fig. 1 and the lattice parameter values in Table 1 and Fig. 5. The fitting model reveals that there is no obvious inclination of the bioaragonite under study from the orthorhombic system (Pmcn).

The unheated bioaragonite unit cell volume 227.36 $Å^3$ exceeds significantly the value of pure aragonite, 226.85 $Å^3$ [21]. The impact of Sr content 1810 ppm, calculated by Lucas-Girot [22], is about 0.06 $Å^3$. The effect of substitution of Na should reduce the expanding effect of Sr in bioaragonite. Thus, the difference should be attributed to the other substitutions in the bioaragonite lattice.

The contraction of the unit cell volume was found to have a sub-linear character and, most likely, to represent two processes of which one ends at a temperature of 250°C and the other begins at a higher temperature. Both effects appeared to be anisotropy and resulted in a diminishing lattice towards vectors *a* and *c* while lattice parameter *b* increased (Fig. 5).

The general shape of the XRD pattern had not changed after the $H_2O_2$ treatment, so it might be concluded that the treatment of the shell matter has not destroyed

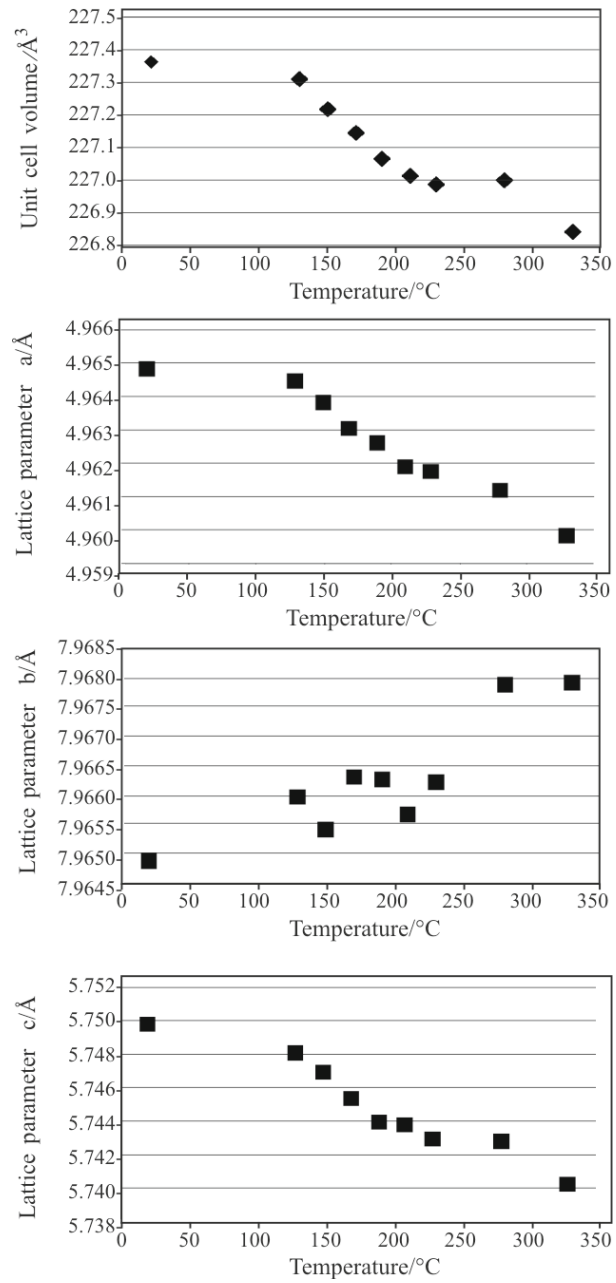


**Fig. 5** Changes in unit cell volume and lattice parameters *a*, *b* and *c* during 1 h of heating

**Table 1** Lattice parameters and unit cell values of heated bioaragonite

| Temp./°C | *a*/Å | *b*/Å | *c*/Å | *V*/Å$^3$ |
|---|---|---|---|---|
| 20 | 4.9648 | 7.9648 | 5.7497 | 227.36 |
| 130 | 4.9644 | 7.9660 | 5.7480 | 227.31 |
| 150 | 4.9638 | 7.9654 | 5.7468 | 227.22 |
| 170 | 4.9630 | 7.9663 | 5.7452 | 227.15 |
| 190 | 4.9626 | 7.9663 | 5.7438 | 227.07 |
| 210 | 4.9619 | 7.9656 | 5.7437 | 227.02 |
| 230 | 4.9617 | 7.9662 | 5.7428 | 226.99 |
| 280 | 4.9611 | 7.9679 | 5.7427 | 227.01 |
| 330 | 4.9598 | 7.9679 | 5.7401 | 226.84 |

the original aragonite plate-like particles [23]. Whereas the organic matrix of the shell is surrounding pure mineral crystallites, it is difficult to assume that the effects described here might be attributed to organic molecules or their radicals, incorporated into the crystal lattice organization as it was reported earlier [6].

On the other hand, the thermal analysis data suggest a more complicated character of changes. The DTG curves confirm a switch to another process at 250°C, hinting at a more complex essence of those. We tend to interpret this phenomenon as a result of the different kinetics of those processes – most likely, the thermally induced processes need more time to have an impact on the bioaragonite crystal lattice. Or, on the contrary, other thermal effects that appeared in the DTG curves (Fig. 2) are not relevant to bioaragonite and might be attributed to the residual organic matter. However, from Fig. 4, it becomes evident that at least the protein component of the organic matrix was successfully removed with peroxide solution.

This idea is supported by the data obtained: the total change in the lattice unit cell volume of studied bioaragonite is about 0.5 Å$^3$. Neither changes in crystallinity nor a rate of anisotropy has been observed during heating. Thus, even if multiple processes take place, partially overlapping and abating each other, the main reason might be attributed to a few changes in bioaragonite crystallochemistry.

On the basis of the FTIR spectra (Fig. 4), it becomes evident that the amount of water and, most likely, its position in the bioaragonite lattice change during heating comparatively smoothly. Discarding the influence of the adsorbed water, which does not affect the recurrence of the crystal lattice, the most plausible reason for this seems to be the participation of structural water in the bioaragonite organization. However, the hydration of aragonite should lower the symmetry of the crystal structure to monoclinic [15], a phenomenon that was not discovered. On the other hand, hydrated aragonite – ikaite – has been reported to be stable only at temperatures below 100°C [15].

The amount of sulphur in peroxide-treated bioaragonite is remarkable (1890 ppm). While the protein component of the organic matrix was apparently successfully removed (Fig. 4), as it is assumed here, a kind of sulphur compound should be involved in the bioaragonite lattice. During heating, the sulphur, freed from the aragonite lattice, reacts with Ca, forming a small amount of anhydrite (Fig. 4). The most fitting form of sulphur containing ion replacing carbonate in the aragonite structure is sulphite. In fact, the IR vibration bands of $CaSO_3$ were not detected. Thus, the participation of sulphur in the constitution of the bioaragonite lattice seems to have a more complex character, also involving water and Na. This idea is supported by anisotropy of thermally induced changes in the bioaragonite lattice (Fig. 5), indicating the planar configuration of the substituting ion, a phenomenon that cannot be explained by the simple incorporation of water into it.

## Conclusions

- Bioaragonite of *T. decussatus* has a specific feature, which appears in expanded unit cell volume in comparison with a theoretical value for 'normal' aragonite with the same Sr content.
- The emission of water and carbon dioxide in 4 overlapping steps and the contraction of the aragonite lattice take place simultaneously at heating *T. decussatus* shells up to 330°C. This transition of bioaragonite has an anisotropy character – the orthorhombic structure remains.
- The anisotropic character of temperature-induced changes in the bioaragonite structure is explained by complex impurities, involving water and sulphur incorporation into the aragonite lattice during the in vivo mineralization process.
- The thermal excitation of bioaragonite at temperatures higher than 330°C results in a transition of the orthorhombic structure into trigonal (calcite). Before the transition, the foregoing changes in the bioaragonite structure take place, lowering the phase-change temperature and obviously triggering it.

## Acknowledgements

This work is supported by ESF Grant No. 7159 and the Nordic Mineralogical Network.

## References


1 H. A. Lowenstam, Science, 211 (1981) 1126.
2 S. N. Golubev, Real'nye kristally v skeletakh kokkolitophorid, Nauka, Moscow 1981, p. 164 (in Russian).
3 J. Peric, M. Vucak, Lj. Brecevic and D. Kralj, Thermochim. Acta, 277 (1996) 175.
4 N. Passe-Coutrin, Ph. N'Guyen, R. Pelmard, A. Ouensanga and C. Bouchon, Thermochim. Acta, 265 (1995) 135.
5 J. Balmain, B. Hannoyer and E. Lopez, J. Biomed. Mater. Res., 48 (1999) 749.
6 B. Pokroy, J. P. Quintana, E. N. Caspi, A. Berner and E. Zolotoyabko, Nat. Mater., 3 (2004) 900.
7 H. Mondange-Dufy, Ann. Chim., 5 (1960) 107.
8 A. Baumer, M. Ganteaume and M. Bernat, Thermochim. Acta, 221 (1993) 255.
9 V. Vongsavat, P. Winotai and S. Meejoo, Nucl. Instrum. Methods Phys. Res. B, 243 (2006) 167.
10 A. A. Finch and N. Allison, Geochim. Cosmochim. Acta, 67 (2003) 4519.
11 B. E. Rosenheim, P. K. Swart, S. Thorrold, P. Willenz, P. Berry and C. Latkoczy, Geology, 32 (2004) 145.
12 Y. Dauphin and A. Denis, Comp. Biochem. Physiol. A, 126 (2000) 367.
13 D. Verma, K. Katti and D. Katti, Spectrochim. Acta, 67 A (2007) 784.
14 G. F. Taylor, Am. Mineral., 60 (1975) 690.
15 K.-F. Hesse and H. Küppers, Z. Kristallogr., 163 (1983) 227.
16 M. Földvári, F. Paulik and J. Paulik, J. Thermal Anal., 33 (1988) 121.
17 NIST/EPA Gas-Phase Infrared Database. www.http://www.nist.gov/srd/nist35.htm.
18 S. A. Howard and K. D. Preston, Rev. Mineral., 20 (1998) 217.
19 X. Bourrat, L. Francke, E. Lopez, M. Rousseau, P. Stempfle, M. Angellier and P. Alberic, Cryst. Eng. Comm., 9 (2007) 1205.
20 R.A. Nyqust, Infrared and Raman Spectral Atlas of Inorganic Compounds and Organic Salts, Vol. 1, Academic Press, San Diego 1997, p. 119.
21 R. Duda and L. Rejl, Phys. Prop. Encyclopedia of Minerals, 2nd Ed. 1990, p. 979.
22 A. Lucas-Girot, O. Hernandez and H. Oudadesse, Mater. Res. Bull., 42 (2007) 1061.
23 H. Mutvei, Palaeontology, 2 (1984) 111.


ICTAC 2008

DOI: 10.1007/s10973-008-9623-9